Theor Chem Acc (2010) 127:519–538
DOI 10.1007/s00214-010-0742-6

REGULAR ARTICLE

An investigation of the lowest reaction pathway of propene + BCl_3 decomposition in chemical vapor deposition process

Xiaoqiong Jiang · Kehe Su · Xin Wang · Yanli Wang · Yan Liu · Qingfeng Zeng · Laifei Cheng · Litong Zhang

Received: 23 December 2009 / Accepted: 1 March 2010 / Published online: 3 April 2010

Abstract The lowest reaction pathway or one of the favored possible paths in the CVD process of preparing boron carbides with BCl_3-C_3H_6(propene)-H_2 precursors was searched theoretically, which involves 95 transition states and 103 intermediates. The geometries of the species were optimized by employing the B3PW91/6-311G(d,p) method. The transition states as well as their linked intermediates were confirmed with frequency and the intrinsic reaction coordinates analyses. The energy barriers and the reaction energies were evaluated with the accurate model chemistry method at G3(MP2) level after a non-dynamical electronic correlation detection. The heat capacities and entropies were obtained with statistical thermodynamics, and the heat capacities were fitted into analytical equations. The Gibbs free energies at 298.15 K for all of the reaction steps were reported. The energies at any temperature could be derived classically by using the analytical heat capacities. All the possible elementary reactions, including both direct decomposition and the radical attacking dissociations, for each reaction step were examined, and the one with the lowest energy or energy barrier was further studied in the next step. It was found that there are 19 reaction steps in the lowest path to produce the final BC_3 cluster including two steps of initializing the reaction chain of producing H and Cl radicals. The highest energy in the lowest reaction pathway is 215.1 kJ/mol at 298.15 K and that for 1,200 K is 275.1 kJ/mol. The results are comparable with the most recent experimental observation of the apparent activation energy 208.7 kJ/mol.

Keywords Pathways · Propene and boron trichloride · Decomposition

Electronic supplementary material The online version of this article (doi:10.1007/s00214-010-0742-6) contains supplementary material, which is available to authorized users.

X. Jiang · K. Su (✉) · X. Wang · Y. Wang · Y. Liu
School of Natural and Applied Sciences,
Northwestern Polytechnical University, Xi'an 710072,
Shaanxi, People's Republic of China
e-mail: sukehe@nwpu.edu.cn

Q. Zeng · L. Cheng · L. Zhang
National Key Laboratory of Thermostructure Composite Materials, Northwestern Polytechnical University,
Xi'an 710072, Shaanxi, People's Republic of China

1 Introduction

Continuous carbon fiber reinforced silicon carbide matrix composite (C/SiC) is one of the most promising structural materials for high temperature applications such as rocket nozzles, aeronautic jet engines and aircraft braking systems [1–5]. However, the matrix cracks produced due to the mismatch of thermal expansion between the fiber and matrix are unavoidable [6]. These cracks generally remain open throughout the application of the material and, consequently, the carbon fibers and pyrolytic carbon (PyC) interface would be consumed by the oxidizing medium. This drawback limits the long-term applications of C/SiC in high-temperature oxidizing environments [3, 4]. The investigation of reliable oxidation-resistant component (or coating) attracted much attention. Boron-containing materials were recognized as one of the most successful oxidation protection systems [7–11]. This is due to that the low viscosity B_2O_3 formed in situ is able to fill the cracks and slow down the in-depth diffusion of moisture and oxygen [3, 12].

The preparation of boron carbides (also denoted as the self-healing materials) was widely conducted [13–20], in

which the temperature chemical vapor deposition (CVD) or chemical vapor infiltration (CVI) is the most privileged method [21]. A number of reactive gaseous mixtures were found available, such as BCl_3/C_6H_6 [22, 23, 26], BCl_3/C_2H_2/[24], BCl_3/C_3H_8 [25], $BCl_3/CH_4/H_2$ [27–30] and BCl_3/C_3H_6(propene)/H_2 [31–34]. Although boron carbide was firstly synthesized by Joly and Hebd [35], attempts to fabricate high quality boron carbide have never stopped. Way et al. [22] and Cermignani et al. [23] deposited B_xC_{1-x} with BCl_3-C_6H_6 gaseous mixtures and obtained a maximum boron content of 15–17 at.%. Derre et al. [24] prepared a boron-doped carbon of 22 at.% boron with BCl_3-C_2H_2 precursors. Jacques et al. [25] deposited BC_x coating of 33 at.% boron with BCl_3-C_3H_8. A detailed study by Kouvetakis et al. [26] revealed that BC_3 could be synthesized with CVD method by using benzene and BCl_3 gases at 800 °C. More experimental and theoretical investigations were carried out with the BCl_3-CH_4-H_2 gaseous system [27–30]. The BCl_3-C_3H_6(propene)-H_2 system also drew much attention in the most recent years [31–34]. Wenbin Yang et al. [31, 32] observed that deposition temperature had great influence on the depositing rates, morphologies and bonding states of B-C coating and the concentration of boron decreased with increasing temperature. Yongsheng Liu et al. [33] reported that a mixture of BCl_3-C_3H_6(propene)-H_2 could be used to fabricate boron-doped carbon coating with the low pressure chemical vapor deposition (LPCVD) technique and found five types of bonding states: B-C, B-sub-C, BC_2O, BCO_2 and B-O. An apparent activation energy of 208.74 kJ/mol below 1,273 K in the system was also reported [33]. In addition to the study of the $BCl_3 + CH_4 + H_2$ system by Yan Zeng et al. [29], Tao Wang et al. [34] in our group carried out a relatively complete theoretical research on the gas phase reaction thermodynamics in the CVD process of preparing boron carbides *via* the precursors of BCl_3-C_3H_6(propene)-H_2.

However, the detailed kinetics (or mechanisms) of the CVD process of preparing boron carbides with BCl_3-C_3H_6(propene)-H_2 precursors has not been reported so far. This is also understandable since the experiments have great difficulties in measuring the intermediates and the transition states (to determine the elementary reactions and their kinetics properties, for example) in the high-temperature system with complicated reactions. The present work will thus develop the lowest reaction pathway of $C_3H_6 + BCl_3 + H_2$ decomposition with theoretical calculations based on the first principles. This includes the determination of the intermediates (IM) [29, 34, 65] and transition states (TS), the connection of the reaction pathways (by examination of the intrinsic reaction coordinates (IRC)), determination of the energies of the species as well as the activations energies with accurate model chemistry method and the determination of the rate control steps.

2 Computational methods and strategy

Density functional theory (DFT), complete active space self-consistent field (CASSCF) and high accurate model chemistry calculations were carried out for the reaction pathways of the $C_3H_6 + BCl_3 + H_2$ system by using the Gaussian-03 program [36]. The geometries of reactants, transition states, intermediates and products were optimized by employing the DFT-B3PW91 [37, 38] method combined with 6-311G(d,p) basis sets. This method was chosen because it was found to reproduce the molecular geometries systematically better than a number of other methods [39, 40]. Frequency analyses at the same level of theory were proceeded with the optimized geometries to determine the harmonic vibrational frequencies, the zero-point energies (ZPE; scaled by 0.9631 [41]) and to confirm the structure being a stationary species or a transition state (i.e., without or with solely an imaginary frequency, respectively). The intrinsic reaction coordinates [42] for both forward and reverse directions started at each TS were also calculated to verify the correct connections.

Since the $C_3H_6 + BCl_3 + H_2$ system is so complicated that it may involve too many reaction paths, intermediates and transition states, an exploration of the complete reaction mechanisms is temporarily unpractical for us. Alternatively, we employed a strategy to examine each reaction step in detail and chose the path with the lowest energy barrier as the feasible path to proceed into the next step. Obviously, this choice cannot promise to identify the global most favorable path of the reaction. This is because that the next step may have a higher barrier than the steps existed in the higher paths of the last step. However, this is probably a practical strategy for a kinetics study of a complicated system, which has not been seen so far. In this way, the further work may systematically examine the next lowest paths.

In determination of the computational methods of the energies, the non-dynamical electronic correlations were firstly examined with CASSCF/6-31G(d,p) calculations [43–48]. The active space was chosen to be (4, 5; i.e., 4 active electrons in 5 active orbitals) for closed and (5,5) for open shell systems. It was found that all of the dominant configuration coefficients are larger than 0.90 except only one for TS35 by 0.87, and the detailed results are listed in Supplement 1. Therefore, a single reference-based method is acceptable in this work. It should be noted that a calculation with the multi-reference configuration interactions even for medium size basis sets needs computational

expenses that exceeds our resources for the $C_3H_6 + BCl_3 + H_2$ system.

The G3MP2 [49, 50] method was thus chosen because it has been widely used [51, 52] in the accurate calculations of molecular energies or reaction energies (e.g., the mean absolute deviation for the G2/97 test set [53, 54] is ±1.30 kcal/mol [49]). This work used the B3PW91/6-311G(d,p) optimized geometries for the G3MP2 energy evaluations.

Heat capacity, entropy, enthalpy and Gibbs free energy of the species at 298.15 K were evaluated with the standard statistical thermodynamics procedures by using the B3PW91/6-311G(d,p) geometries and frequencies. The heat capacities as a function of temperature in 200–2,000 K were also developed with the same method and fitted into an analytical equation (Eq. 1). By using the heat capacities, the energy and the energy barriers at any temperature (e.g., 1,200 K, a temperature close to the generally adopted reaction condition [20, 55–59]) were derived classically.

3 Results and discussion

3.1 Structure and vibrational frequencies

A total number of 103 intermediates and 95 transition states associated with the singlet, doublet and triplet potential energy surfaces are involved. The structure, symmetry and electronic state are shown in Fig. 1 (in the alphabetic order of C-H-B-Cl for IM's and TS's). The Cartesian coordinates are listed in Supplement 2 and will be used in the high temperature heat capacity and entropy evaluations in the rotational partition function calculations. The vibrational frequencies are listed in Supplement 3 and will be used in the evaluation of the vibrational partition functions.

3.2 Energies

The energies ($U_{0\ K}$), standard enthalpies ($H_{298.15\ K}$) and Gibbs free energies ($G_{298.15\ K}$) obtained with G3(MP2) combined with standard statistical thermodynamics are listed in Supplement 4. The activation energies and reaction energy changes, including enthalpies, entropies and Gibbs free energies, for the 95 transition states associated reactions as well as the reactions without transition state at 298.15 K are listed in Supplement 5. The standard molar heat capacity $C^{\theta}_{p,m}$ and entropy S^{θ}_{m} are calculated statistically with the ideal gas model. The results for 298.15 K are listed in Supplement 6. In order to simplify the applications of the high-temperature entropy, enthalpy and Gibbs free energy evaluations, polynomial fit of the theoretical heat capacities are carried out within 200–2,000 K. The data are fitted into Eq. 1 (consistent with the form of Ref. 60), and the results are listed in Supplement 7.

$$C^{\theta}_{p,m} = a_0 + a_1 T + a_2 T^2 + a_3 T^3 + a_4 T^{-2} \quad (1)$$

As shown in Supplement 7, all of the correlation coefficients are larger than 0.999 except that, 0.9989 for BCl_2, representing that the fit is very accurate. When compared with the available experiments [60–64] as shown in Table 1, the enthalpies of formation and the Gibbs free energies of formation for the stable intermediates [29, 65] are generally in very good agreements. The deviations for C_3H_6, C_3H_5, CH_3Cl, CH_4, CH_3, BCl_3, HCl and H_2 are within 10 kJ/mol. Large deviation is in BCl_2 possibly due to a questionable experimental data in Refs. [60], [61] and [63], but it is consistent with Ref. 64 as presented in Ref. [29].

3.3 Reaction pathways of $C_3H_6 + BCl_3$ decomposition

The potential energy profile diagrams obtained using the relative Gibbs free energies (in kJ/mol) at 298.15 K at G3(MP2)//B3PW91 level are illustrated in Figs. 2, 3, 4, 5, 6, 7, 8, 9, 10, 11, 12, 13, 14, 15, 16, 17, 18 and 19. All the reactions linked in the figures are spin consistent or are consistent with the Wigner–Witmer rules [66] except for the homogenous bond-cleavage in the singlet surface. Figure 2 illustrates all of the possible intermolecular reaction paths of the reactants $C_3H_6 + BCl_3$. Figure 3 shows all the possible decompositions of the adduct IM99 produced *via* the lowest barrier path in the last step. Figs. 4 5, 6, 7, 8, 9, 10, 11, 12, 13, 14, 15, 16, 17 and 18 express the decomposition of the further intermediates found with the same strategy (as presented in Sect. 2). Figure 19 is the proposal of the final lowest reaction pathways. It should be noted that some of the pure thermodynamic processes (i.e., the process in which a TS is unable to be located in the radical attacking reactions) are not shown in the figures,

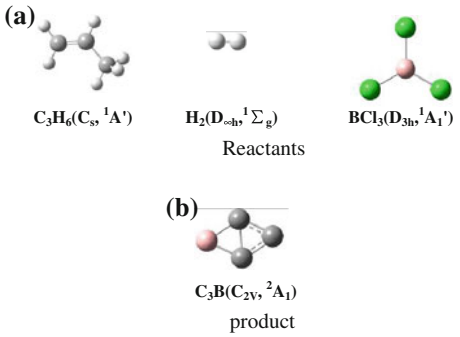

Fig. 1 Structure, symmetry and electronic state of the reactants, product, intermediates and transition states in the $C_3H_6 + BCl_3 + H_2$ system obtained with B3PW91/6-311G(d,p) (listed in the alphabetic order of C-H-B-Cl)

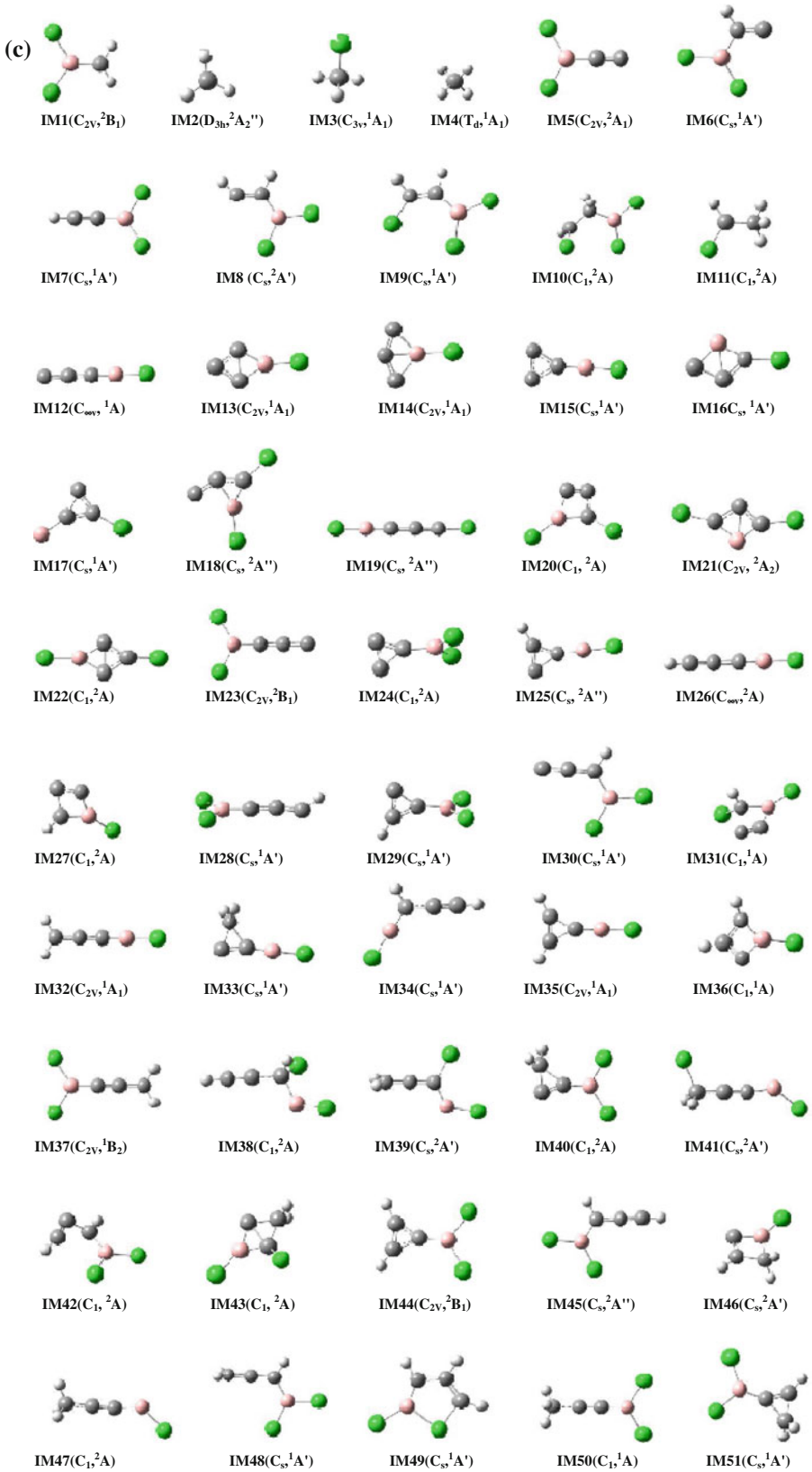

Fig. 1 continued

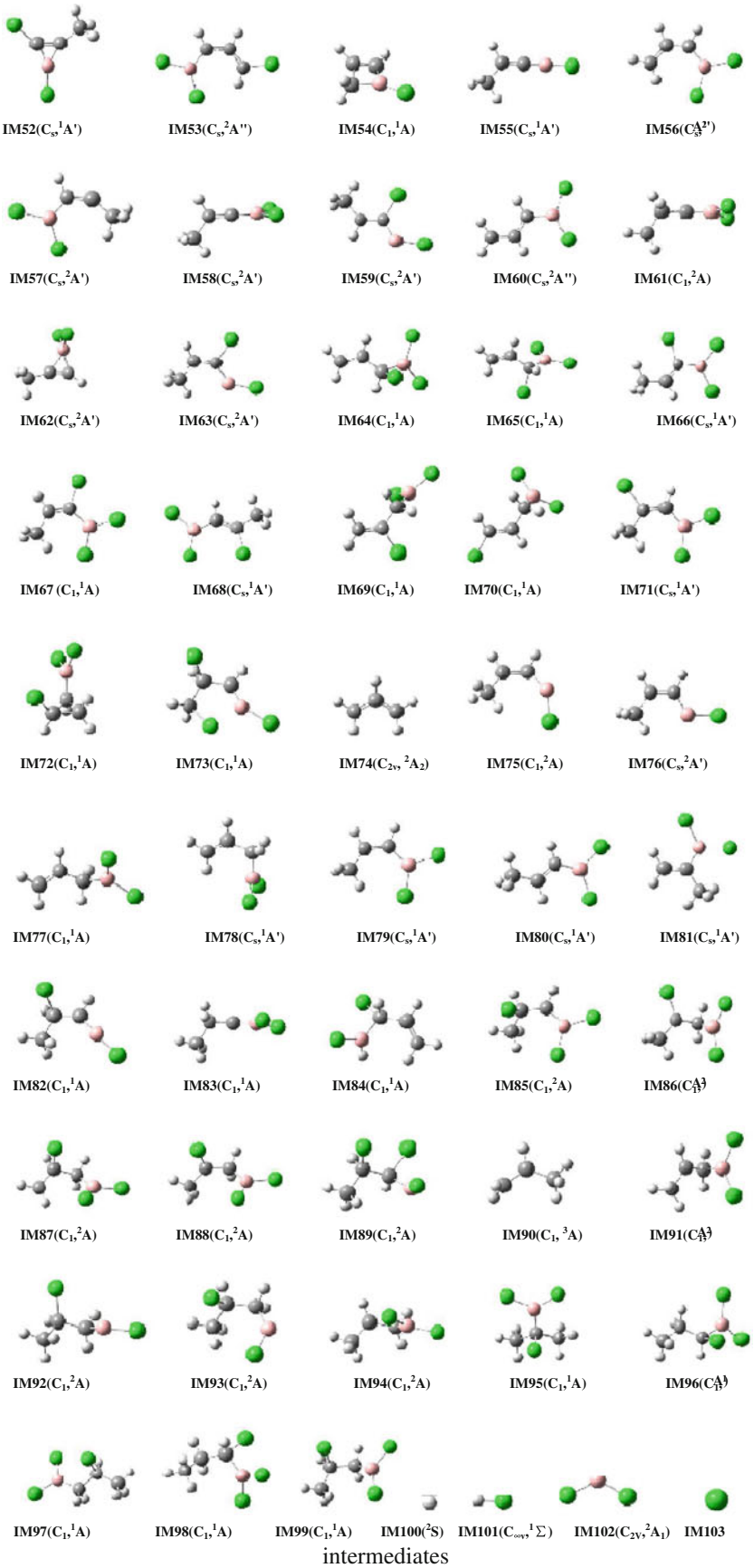

Fig. 1 continued

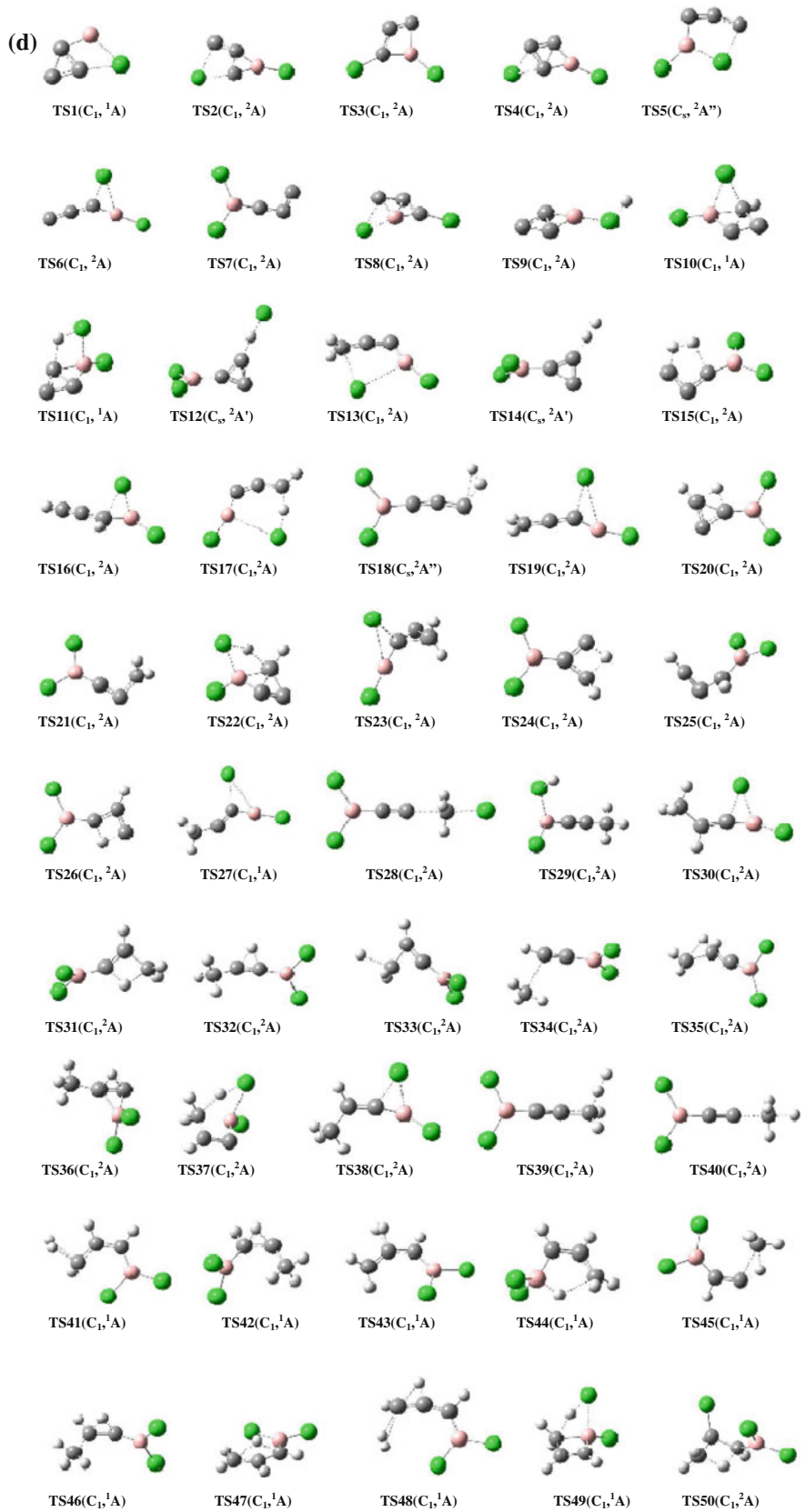

Fig. 1 continued

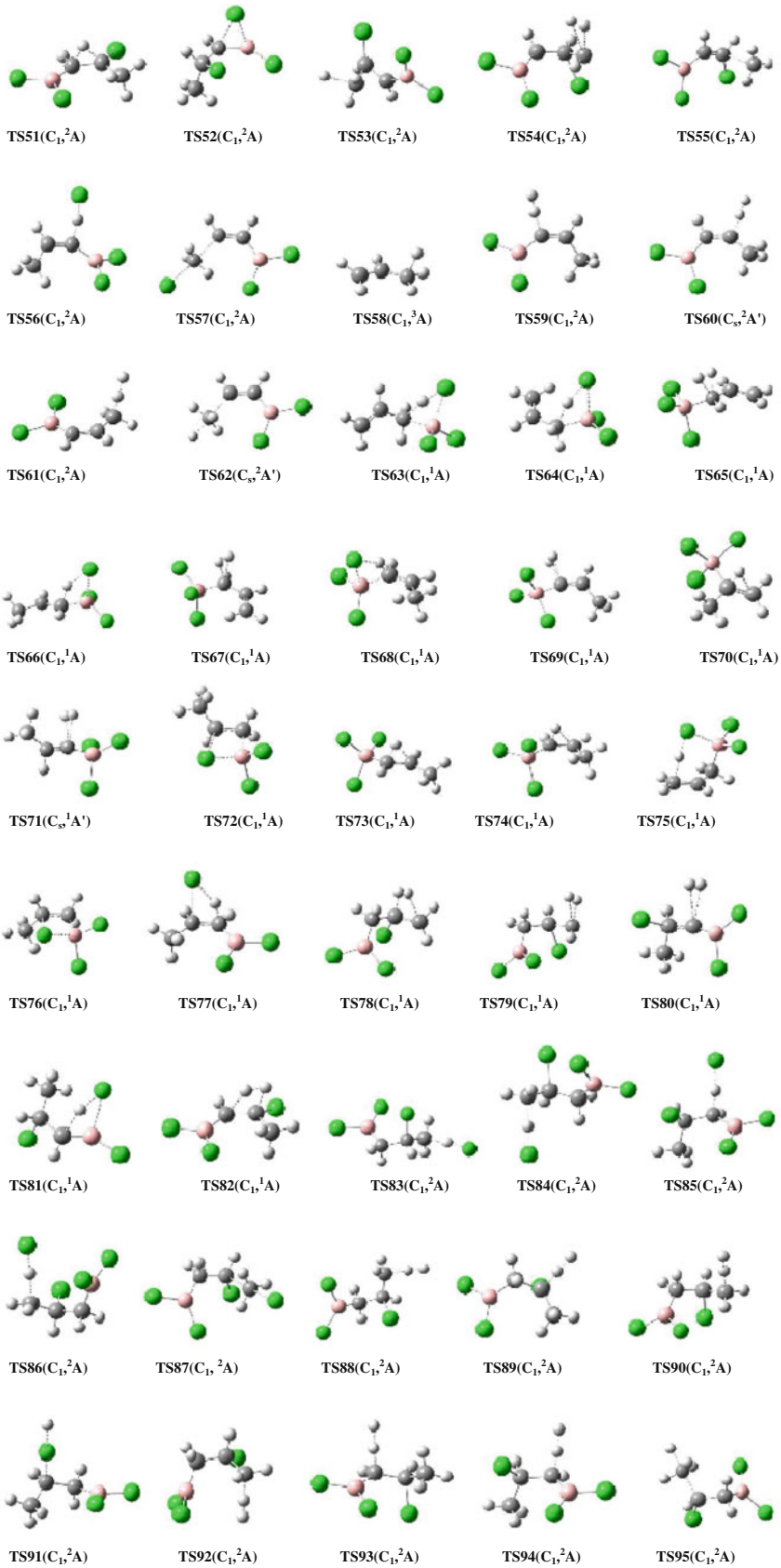

Fig. 1 continued

Table 1 Standard enthalpies of formation $\Delta_f H_m^\theta$ (298.15 K) and Gibbs free energies of formation $\Delta_f G_m^\theta$ (298.15 K) predicted [29, 65] with G3(MP2) and the comparisons with available experiments

Species (symmetry, state)	$\Delta_f H_m^\theta$ (298.15 K; kJ/mol)		$\Delta_f G_m^\theta$ (298.15 K; kJ/mol)	
	G3(MP2)	Exp.	G3(MP2)	Exp.
$C_3H_6(C_s,{}^1A')$	18.9	19.70 ± 1.10[a]	53.3	
		20.0[c]		
		20.2[d]		
C_3H_5 ($C_{2v},{}^2A_2$)	166.9	171.00 ± 3.00[a]	183.4	
		161[d]		
$H_2(D_{\infty h},{}^1\Sigma_g)$	−4.7	0	−4.6	0
$CH_4(T_d,{}^1A_1)$	−74.3	−74.60 ± 0.30[a]	−53.0	−50.768[b]
		−74.873 ± 0.34[b]		−50.5[c]
		−74.6[c]		
		−74.5 ± 0.4[d]		
$CH_3(D_{3h},{}^2A_2'')$	143.4	146.30 ± 0.50[a]	141.5	147.950[b]
		145.687 ± 0.80[b]		147.9[c]
		145.7[c]		
		145.8 ± 1[d]		
$BCl_3(D_{3h},{}^1A_1')$	−412.5	−403.0 ± 2.1[a]	−394.6	−387.969[b]
		−403.0 ± 2.1[b]		−388.7[c]
		−403.8[c]		
		−404[d]		
		−412.54[e]		
$BCl_2(C_{2v},{}^2A_1)$	−35.4	−79.50[a]	−46.7	−92.544[b]
		−79.50 ± 12.6[b]		
		−83 ± 63[d]		
		−28.45[e]		
$CH_3Cl(C_{3v},{}^1A_1)$	−82.9	−81.87 ± 0.60[a]	−56.3	−60.146[b]
		−83.68 ± 2.1[b]		
		−81.9[c]		
		−82.0 ± 0.5[d]		
$HCl(C_{\infty v},{}^1\Sigma)$	−93.9	−92.31 ± 0.10[a]	−96.0	−95.300[b]
		−92.312 ± 0.21[b]		−95.3[c]
		−92.3[c]		

[a] Ref. [60]
[b] Ref. [61]
[c] Ref. [62]
[d] Ref. [63]
[e] Ref. [64]

neither will be discussed. The concentration distribution of these species can be found in the thermodynamics investigations [34].

3.3.1 Initial reactions

In the system of preparing B_xC_y with $C_3H_6 + BCl_3 + H_2$ precursors, the initial formation of B-C bond or B-C_n structures should be emphasized. Figure 2 illustrates the paths of the intermolecular reactions of $C_3H_6 + BCl_3$. It is shown that there are fourteen reaction paths to form the B-C bond within four different types of reactions: (1) the addition of BCl_3 into the C=C bond, (2) Cl shifts onto propene associated with the formation of B-C bond, (3) the release of HCl and (4) the release of H_2.

The lower energy steps are in the first type of reactions. These are the addition of BCl_3 into the C=C bond to form IM99 and IM97 *via* TS76 and TS72 with energy barriers of

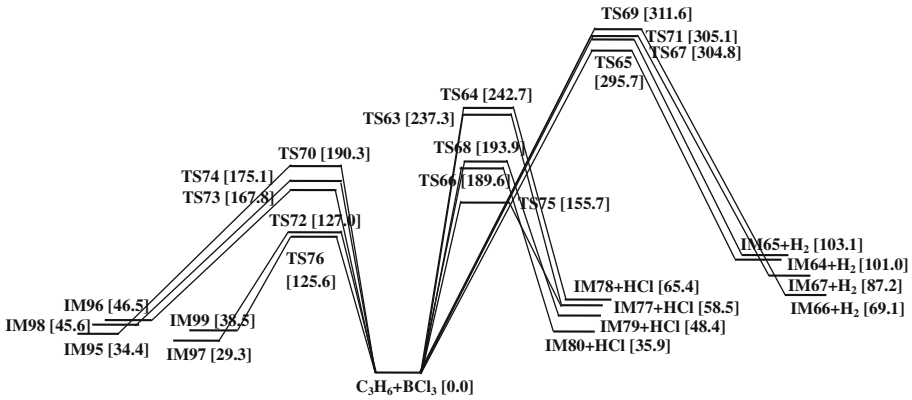

Fig. 2 Initial reaction pathways of $C_3H_6 + BCl_3$. Data in the square brackets are the 298.15 K relative Gibbs free energies (in kJ/mol) obtained at G3(MP2)//B3PW91 level

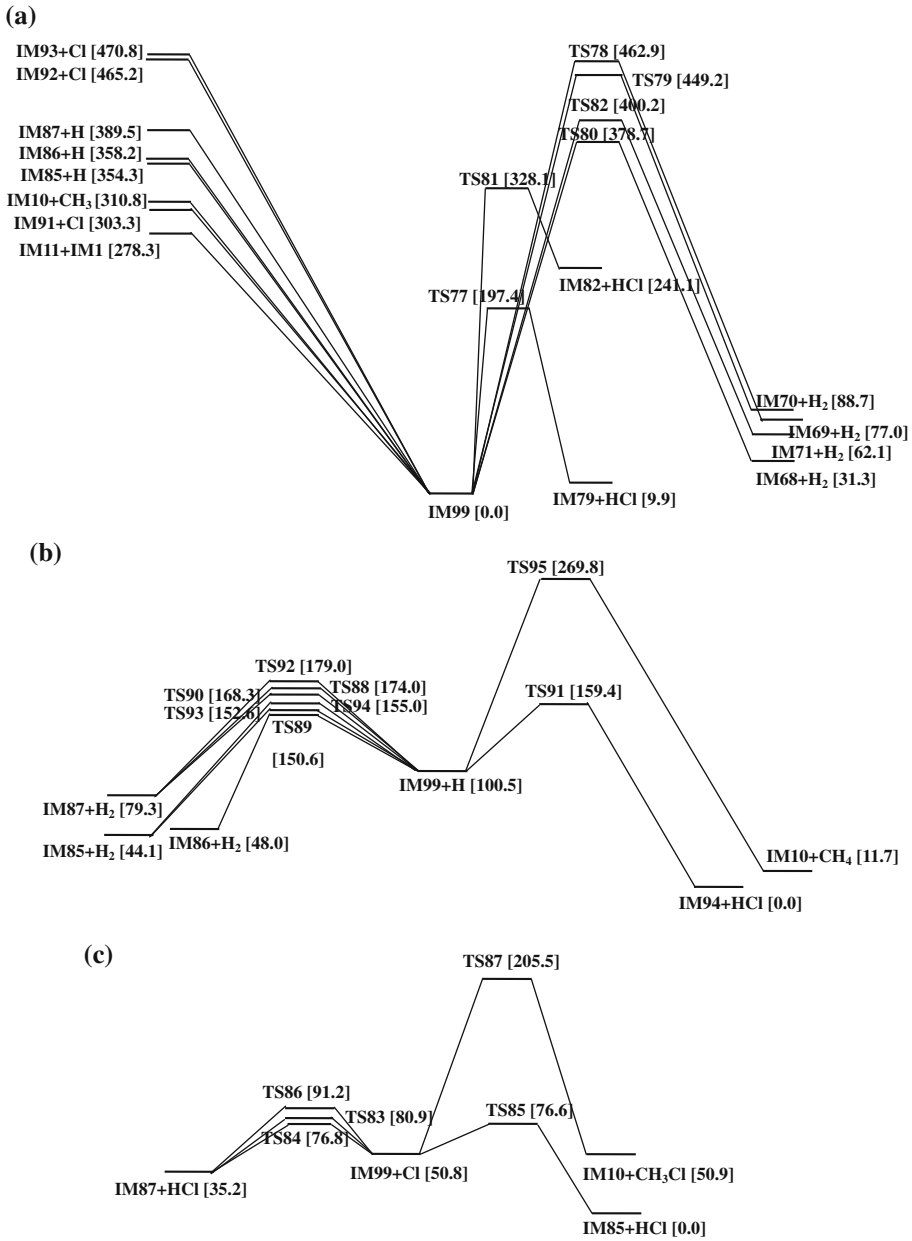

Fig. 3 Direct and indirect (*via* free radical attacking) decomposition pathways of $CH_3CHClCH_2BCl_2$ (IM99). Data in the square brackets are the 298.15 K relative Gibbs free energies (in kJ/mol) obtained at G3(MP2)//B3PW91 level. **a** is for the direct decomposition of IM99. **b** is for the paths of IM99 attacked by a hydrogen radical. **c** is for the paths of IM99 attacked by a chlorine radical

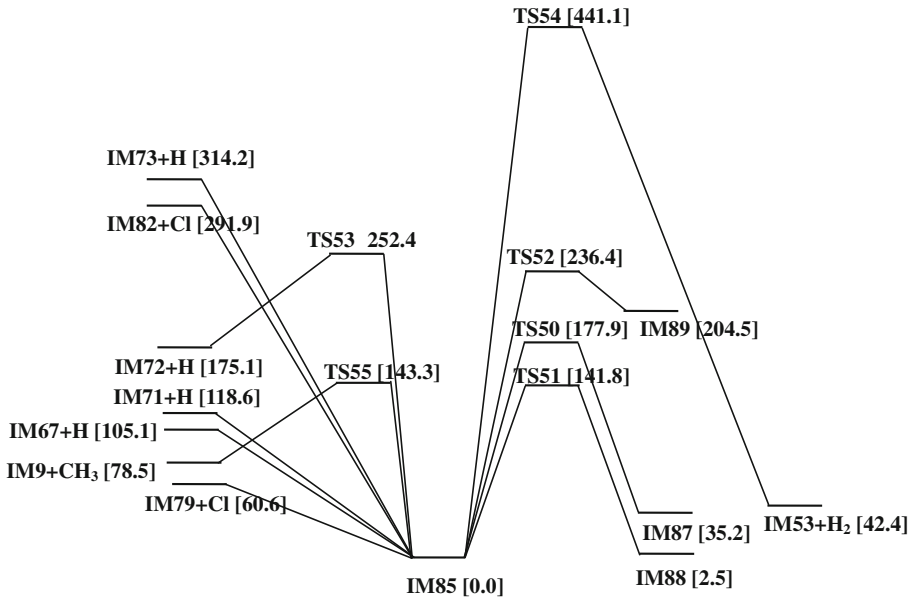

Fig. 4 Decomposition reaction pathways of IM85 radical. Data in the square brackets are the 298.15 K relative Gibbs free energies (in kJ/mol) obtained at G3(MP2)//B3PW91 level

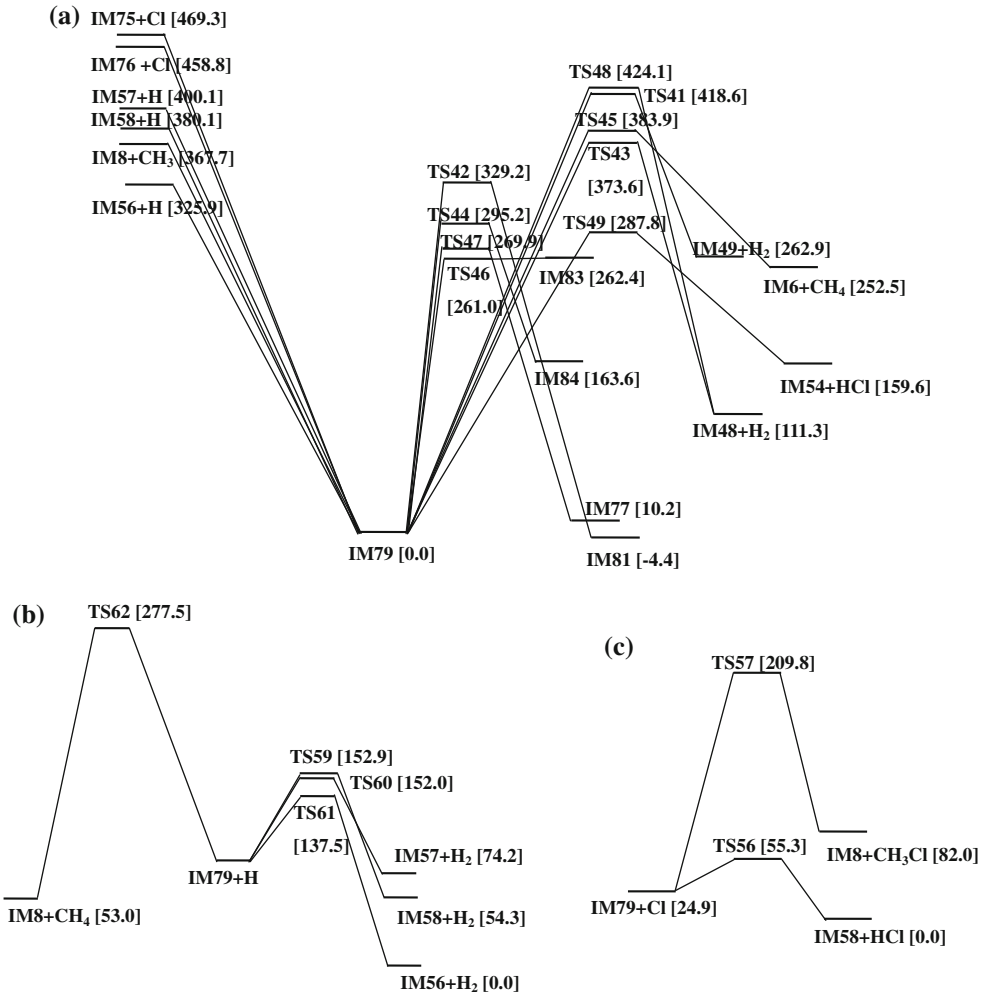

Fig. 5 Direct and indirect (*via* free radical attacking) decomposition pathways of $CH_3CHCHBCl_2$ (IM79). Data in the *square brackets* are the 298.15 K relative Gibbs free energies (in kJ/mol) obtained at G3(MP2)//B3PW91 level. **a** is for the direct decomposition of IM79. **b** is for the paths of decomposition of IM79 attacked by hydrogen radical. **c** is for the paths of decomposition of IM79 attacked by chlorine radical

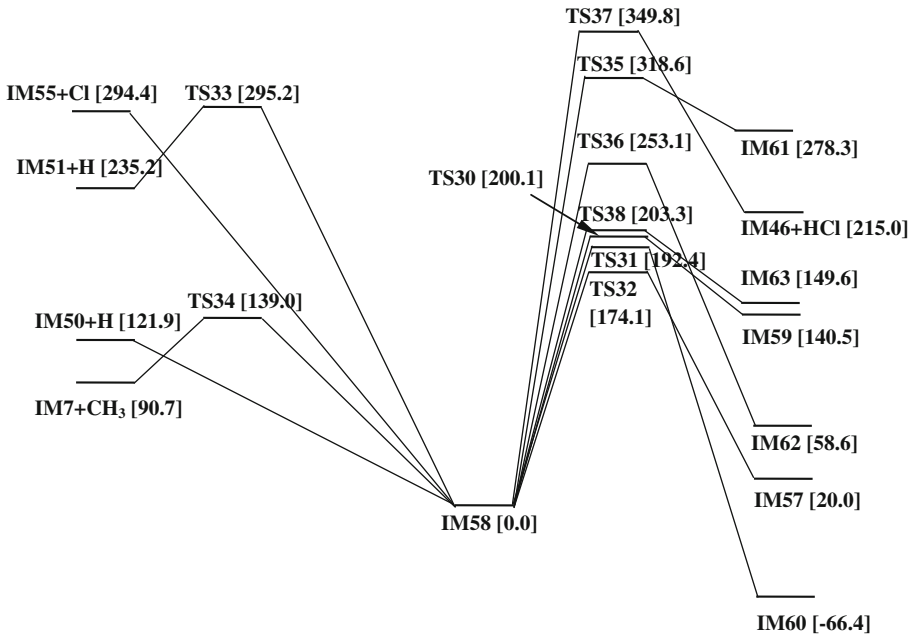

Fig. 6 Decomposition reaction pathways of IM58 radical. Data in the *square brackets* are the 298.15 K relative Gibbs free energies (in kJ/mol) obtained at G3(MP2)//B3PW91 level

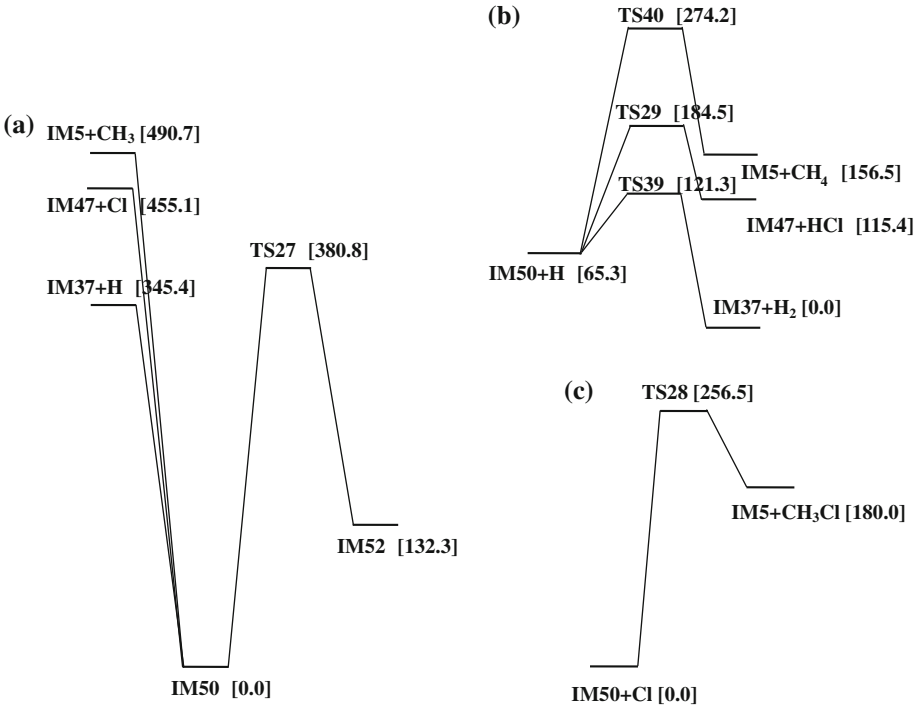

Fig. 7 Direct and indirect (*via* free radical attacking) decomposition pathways of CH_3CCBCl_2 (IM50). Data in the *square brackets* are the 298.15 K relative Gibbs free energies (in kJ/mol) obtained at G3(MP2)//B3PW91 level. **a** is for the direct decomposition of IM50. **b** is for the paths of decomposition of IM50 attacked by hydrogen radical. **c** is for the paths of decomposition of IM50 attacked by chlorine radical

125.6 and 127.0 kJ/mol, respectively. Actually, IM99 and IM97 are conformational isomers with respect to the internal C-B bond rotation. For the complicated reaction system, the study of the subsequent decompositions of the slightly higher path of TS72 → IM97 is a further work for us. It should also be noted that there is a chiral C atom in either IM97 or IM99 associated with TS72 and TS76. Figure 2 shows the structure of the (R)-IM99 and the (S)-IM97. The decomposition paths of the corresponding enantiomers (S)-IM99 and (R)-IM97 are identical and will not be discussed repeatedly. The intermediate IM99 in the lowest energy path of reactants → TS76 → IM99 is thus the reactant of the next step of our interests.

For type (2), a Cl atom shifts onto the middle or the terminal C atom of propene associated with the B atom binding onto the same C atom to produce IM96, IM98 and

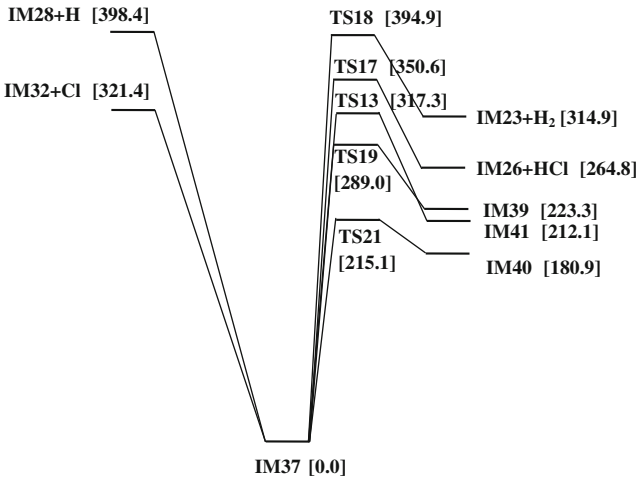

Fig. 8 Decomposition reaction pathways of IM37 radical. Data in the *square brackets* are the 298.15 K relative Gibbs free energies (in kJ/mol) obtained at G3(MP2)//B3PW91 level

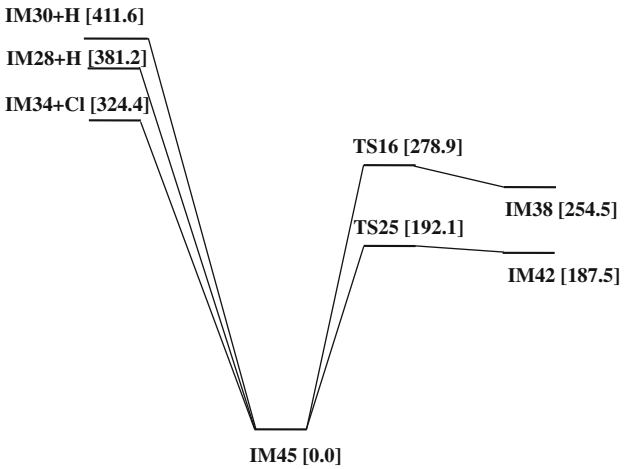

Fig. 11 Decomposition reaction pathways of IM45 radical. Data in the *square brackets* are the 298.15 K relative Gibbs free energies (in kJ/mol) obtained at G3(MP2)//B3PW91 level

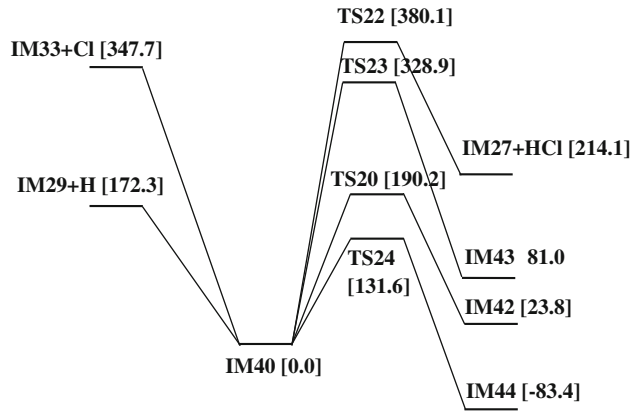

Fig. 9 Decomposition reaction pathways of IM40 radical. Data in the *square brackets* are the 298.15 K relative Gibbs free energies (in kJ/mol) obtained at G3(MP2)//B3PW91 level

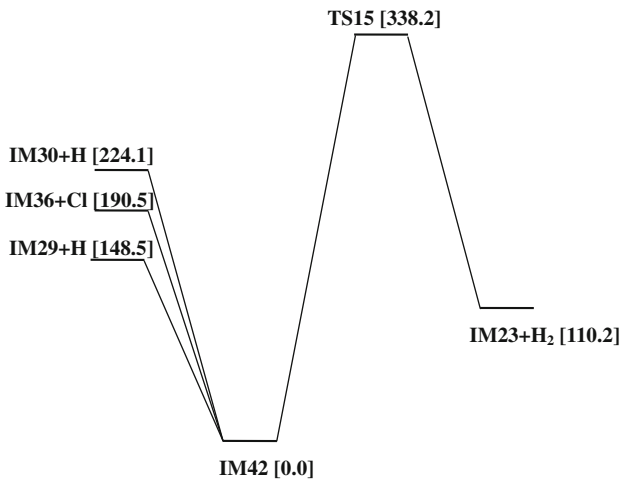

Fig. 12 Decomposition reaction pathways of IM42 radical. Data in the *square brackets* are the 298.15 K relative Gibbs free energies (in kJ/mol) obtained at G3(MP2)//B3PW91 level

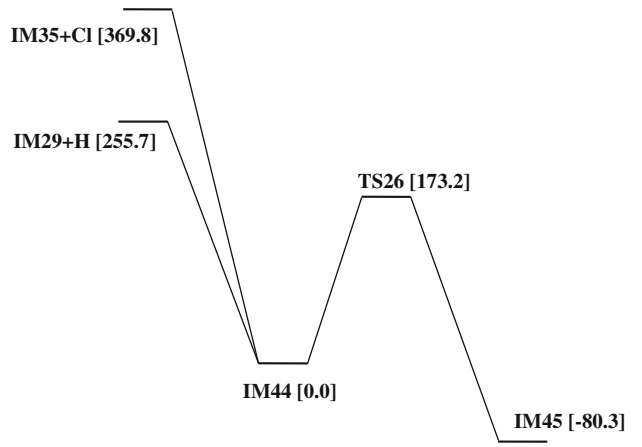

Fig. 10 Decomposition reaction pathways of IM44 radical. Data in the *square brackets* are the 298.15 K relative Gibbs free energies (in kJ/mol) obtained at G3(MP2)//B3PW91 level

IM95 *via* TS73, TS74 and TS70 with energies of 167.8, 175.1 and 190.3 kJ/mol, respectively. These barriers are moderate for the gas phase reactions especially at higher temperatures. The respective reaction paths should also be a further work for us. Type (3) is for the release of an HCl molecule. There are five different paths to produce IM77, IM80, IM79, IM77 and IM78 *via* TS75, TS66, TS68, TS63 and TS64 with 155.7, 189.6, 193.9, 237.3 and 242.7 kJ/mol, respectively. In these paths, IM77 could be produced *via* either TS63 or TS75. The energy values show that the release of an HCl molecule is also moderate for the reactions. For type (4), a molecular H_2 can be dissociated from one C atom of propene either at its $–CH_3$ or $= CH_2$ terminal to form IM64, IM65, IM66 and IM67 *via* TS65, TS67, TS69 and TS71 with energy barriers of 295.7, 304.8,

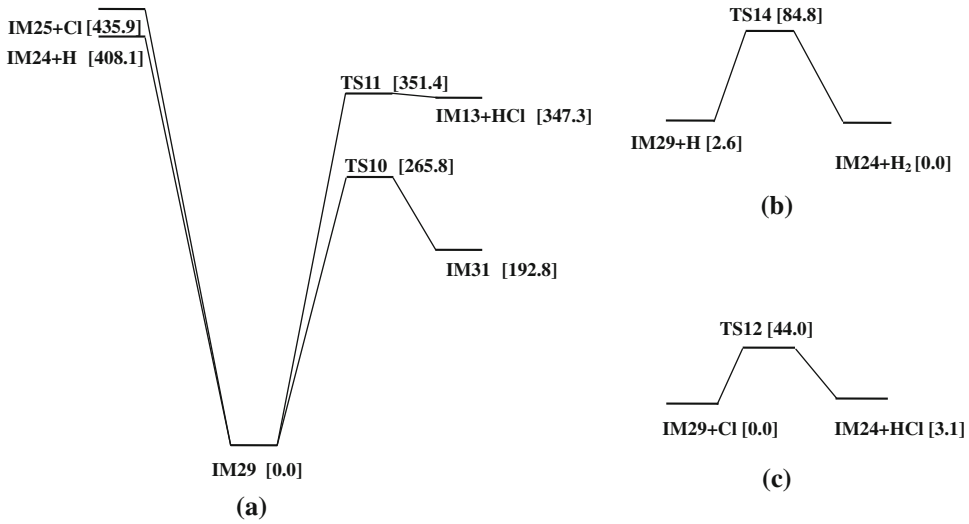

Fig. 13 Direct and indirect (*via* free radical attacking) decomposition pathways of C_3HBCl_2 (IM29). Data in the *square brackets* are the 298.15 K relative Gibbs free energies (in kJ/mol) obtained at G3(MP2)//B3PW91 level. **a** is for the direct decomposition of IM29. **b** is for the path of decomposition of IM29 attacked by hydrogen radical. **c** is for the path of decomposition of IM29 attacked by chlorine radical

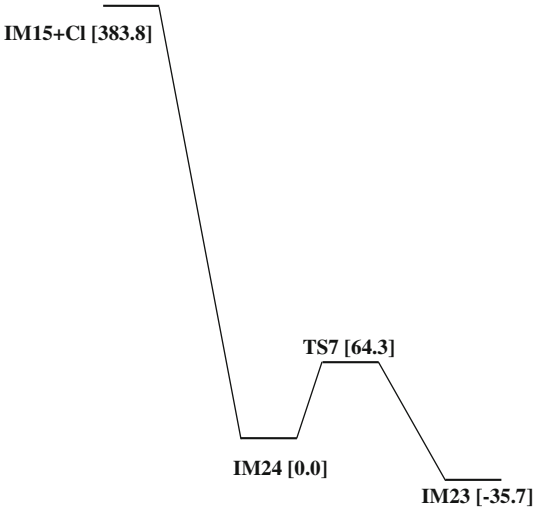

Fig. 14 Decomposition reaction pathways of IM24 radical. Data in the *square brackets* are the 298.15 K relative Gibbs free energies (in kJ/mol) obtained at G3(MP2)//B3PW91 level

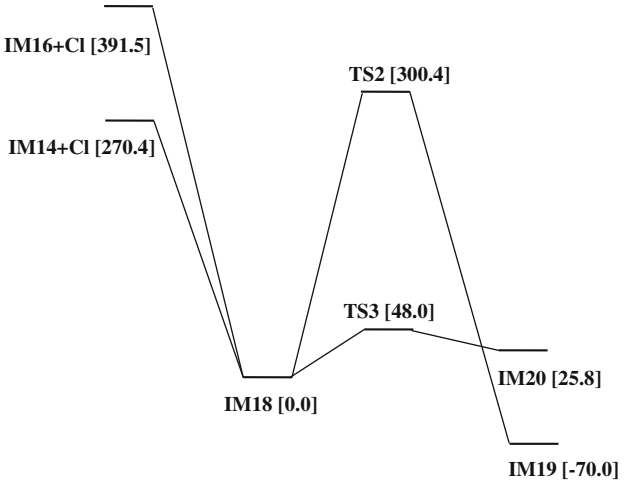

Fig. 16 Decomposition reaction pathways of IM18 radical. Data in the *square brackets* are the 298.15 K relative Gibbs free energies (in kJ/mol) obtained at G3(MP2)//B3PW91 level

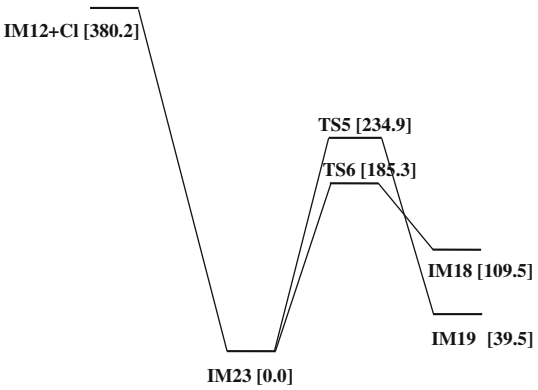

Fig. 15 Decomposition reaction pathways of IM23 radical. Data in the *square brackets* are the 298.15 K relative Gibbs free energies (in kJ/mol) obtained at G3(MP2)//B3PW91 level

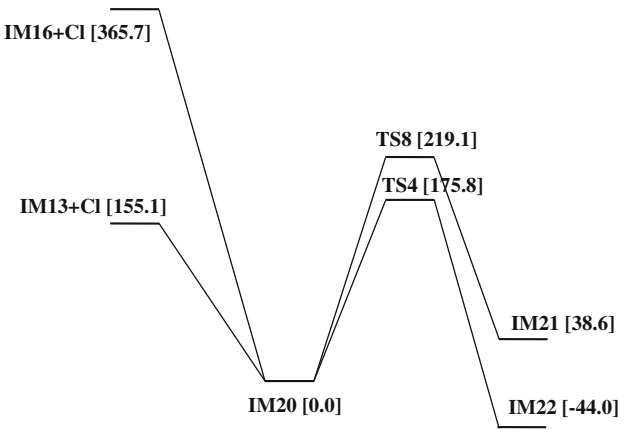

Fig. 17 Decomposition reaction pathways of IM20 radical. Data in the *square brackets* are the 298.15 K relative Gibbs free energies (in kJ/mol) obtained at G3(MP2)//B3PW91 level

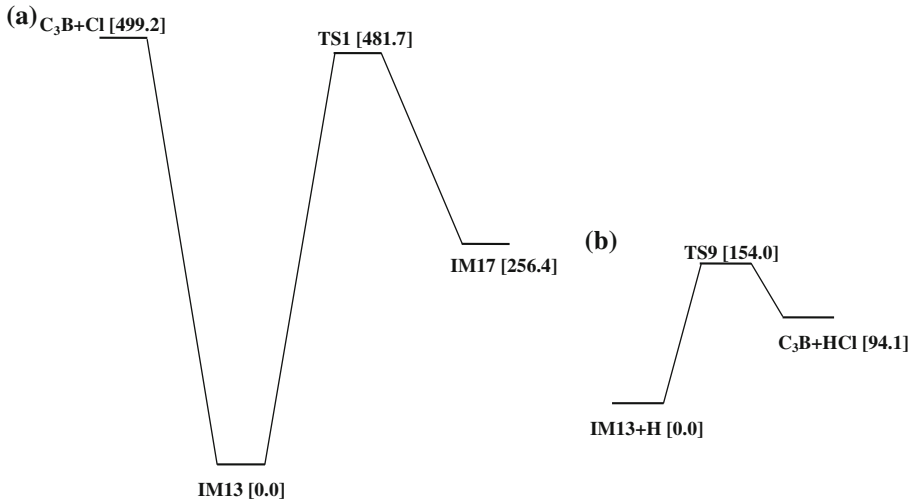

Fig. 18 Direct and indirect (*via* free radical attacking) decomposition pathways of C_3BCl (IM13). Data in the *square brackets* are the 298.15 K relative Gibbs free energies (in kJ/mol) obtained at G3(MP2)//B3PW91 level. **a** is for the direct decomposition of IM13. **b** is for the paths of decomposition of IM13 attacked by hydrogen radical

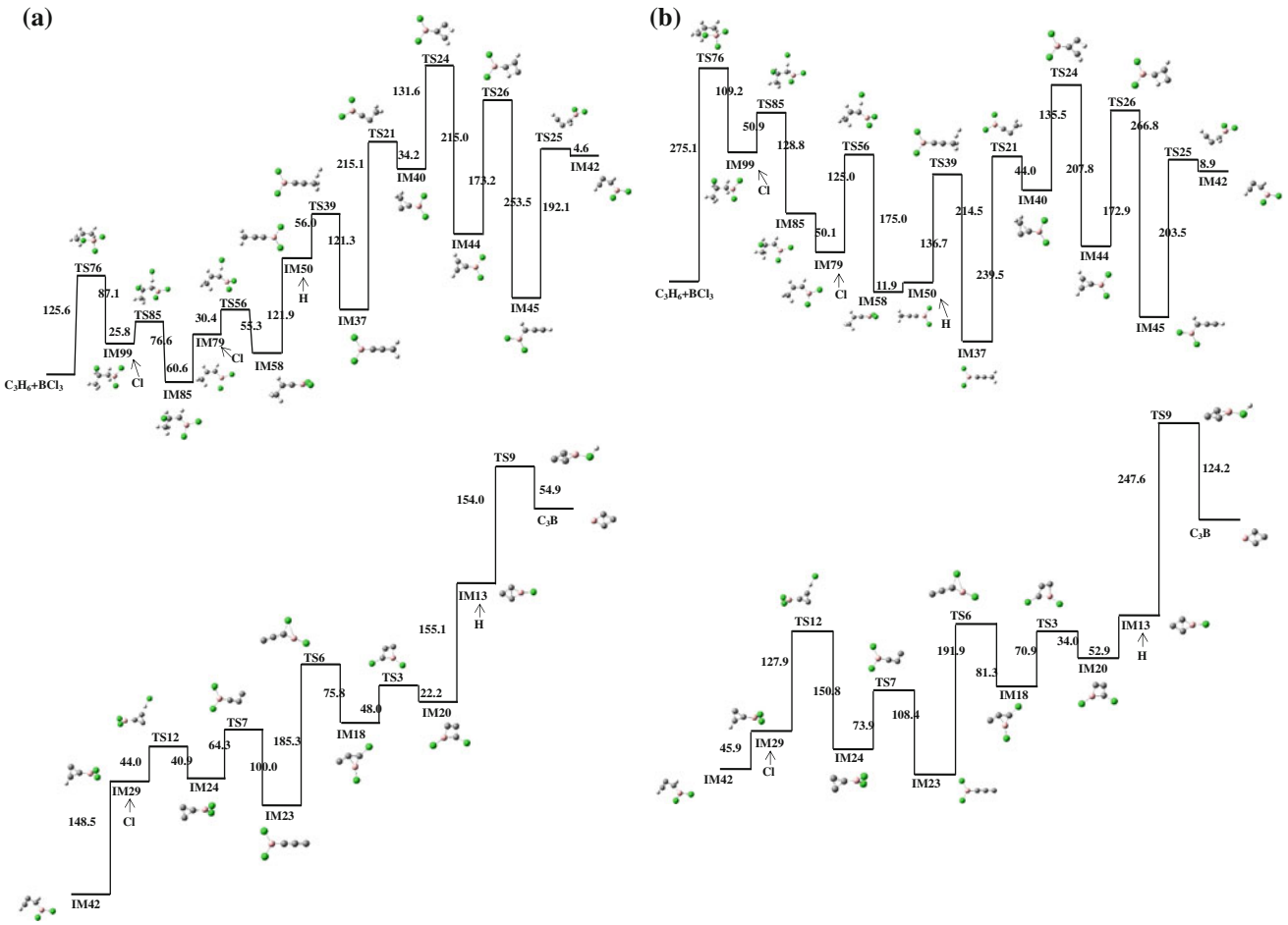

Fig. 19 Proposal of the final lowest reaction pathways of $C_3H_6 + BCl_3$ pyrolysis. Data in the path are the relative Gibbs free energies (in kJ/mol) obtained at G3(MP2)//B3PW91 level. **a** is for the reaction pathways at 298.15 K and **b** is for those at 1,200 K

311.6 and 305.1 kJ/mol, respectively. The energies are obviously higher than the other types of reactions, predicting that these reaction pathways are relatively unfeasible. The branching ratios of the reaction rate, if approximately estimated with the Boltzmann's factor $\alpha = \exp[-(E_1 - E_2)/RT]$, are 1.8, 1.9×10^5 and 2.5×10^7 for the lowest barrier reaction *via* TS76 with respect to the next lowest energy paths *via* TS72, TS75 and TS73, respectively.

3.3.2 Decomposition of IM99 intermediate

Figure 3 presents the decomposition paths of the intermediate $CH_3CHClCH_2BCl_2$ (IM99) produced in the lowest energy path of the initial reactions (Fig. 2). Figure 3a is for the direct decompositions, and there are three different types of reactions: (1) the dissociation of an HCl molecule, (2) the dissociation of a molecular H_2 and (3) the homogenous bond-cleavages. The production of propylene-boron-dichloride (IM79) by decomposing the HCl from the middle of the CCCB chain of IM99 *via* TS77 with an energy of 197.4 kJ/mol is a low energy path lying 130.7 kJ/mol below TS81 of producing IM82. Other types of reactions need much higher energies. The rate branching ratio for the low energy path is 1.5×10^{14} with respect to the next low one. However, the gaseous phase reactions at higher temperatures should follow radical mechanisms. For example, Qu et al. [67] in our group examined the reaction paths of propene pyrolysis and reported that the most favorable paths are mainly in the radical attacking chain reactions. In that work, the authors suggested that the initial production of an H atom could be the ground state propene(X^1A') exciting into its lowest triplet state(a^3A) with an energy of 270.2 kJ/mol and then conducting a bond-cleavage to produce an H atom with an energy of 148.7 kJ/mol. This also applies to the present work because propene is one of the reactants of this work. The initial production of a Cl radical needs an energy of 303.3 kJ/mol if it is produced by the decomposition of IM99 (into IM91 + Cl) as shown in Fig. 3a or that of 454.7 kJ/mol if decomposed from the BCl_3 precursor (an experimental value of 400.7 kJ/mol for the decomposition of $BCl_3 \rightarrow BCl_2 +$ Cl can be obtained by using the data from the NIST-JANAF Tables [61], but the data for BCl_2 is questionable [29]). The energy, 303.3 kJ/mol, is moderate for an initialization of a reaction chain. Subsequently, the H and Cl radical attaching reactions are shown in Fig. 3b, c.

Figure 3b shows the decomposition paths for IM99 attacked by an H radical at different sites. A Cl, H atom or the $–CH_3$ group in IM99 could be dissociated. The energies are much smaller compared to the direct decompositions. On the left hand side, three radicals IM86, IM85 and IM87 and a molecular H_2 from each are produced. The low energy path is for the H on the middle C being decomposed *via* TS89 with an energy of 50.1 kJ/mol. The next lower paths (*via* TS93, TS94, TS90, TS88 and TS92) lie a few kilojoules higher in energy, corresponding to the rate branching ratios of 2.2, 5.9, 1.3×10^3, 1.3 and 9.5×10^4. It is also shown that the decomposition of a Cl atom on the C atom needs a small energy of 58.9 kJ/mol *via* TS91 to produce IM94 and an HCl molecule. The only higher energy path is the decomposition of a CH_3 group to produce IM10 and a methane molecule *via* TS95 with an energy of 169.3 kJ/mol. Therefore, all the lower energy decomposition paths are possible if there is no other even lower energy path.

However, Fig. 3c shows that the decomposition of an H atom in IM99 attacked by a Cl atom needs an energy not more than 41 kJ/mol (or 10 kcal/mol) except for the terminal CH_3 group in IM99 being dissociated *via* TS87 with a higher energy of 154.7 kJ/mol. The release of an HCl molecule for breaking the C–H bond on the terminal CH_3 group of IM99 will produce IM87 *via* TS84, TS83 and TS86 with energies of 26.0, 30.2 and 40.5 kJ/mol, respectively. The dissociation of the H atom on the carbon linking BCl_2 terminal will also produce an HCl molecule and IM85 *via* TS85 with 25.8 kJ/mol, which is the lowest energy path in the present reaction step. It should be noted that TS85 lies only 0.2 kJ/mol lower than TS84 and the product IM85 is more stable than IM87 by 35.2 kJ/mol. The rate branching ratios for the reactions in Fig. 3c are 1.1, 5.7, 3.6×10^2 and 3.6×10^{22}. Compared with the low energy path of H attacking reaction in Fig. 3b, the lowest path of Cl attacking reaction in Fig. 3c has a rate branching ratio of 1.8×10^4. Therefore, the radical IM85 should be considered as the reactant of the next reaction step although IM87 produced here *via* TS84 should have a similar concentration in the reaction system.

3.3.3 Decomposition of IM85 radical

As shown in Fig. 4, the decomposition of IM85 has three types of reactions: (1) the dissociation of a radical (H, Cl or CH_3), (2) intra-molecular H or Cl shift, (3) the release of a H_2 molecule. Among which, the lowest energy path is IM85 decomposing into IM79 and a Cl atom without passing transition state. The energy is 60.6 kJ/mol. Other six pathways to dissociate the H, Cl and CH_3 radicals have energies or energy barriers at least 44.5 kJ/mol higher. In the reaction of intra-molecular H or Cl shift, IM88 corresponds to the H atom on the middle C shifting onto the C linking B (*via* TS51). The energy barrier is 141.8 kJ/mol. The reactant IM85 and IM87 are isomers produced from the 1–3 H shift linked by TS50 with an energy barrier of 177.9 kJ/mol. IM85 can also transform into IM89 by a Cl atom shifting onto the neighboring C atom with a barrier of 236.4 kJ/mol. However, these reactions need energies higher (at least 81.2 kJ/mol) than the lowest path. The release of a H_2 molecule from the terminal CH_3 group of IM85 to form IM53 *via* TS54 needs an extraordinarily high energy of 441.1 kJ/mol. Therefore, IM79 is considered as the reactant of the next step.

3.3.4 Decomposition of IM79 intermediate

Figure 5 presents the decomposition paths of the intermediate $CH_3CHCHBCl_2$ (IM79). Figure 5a is for the direct

decomposition. It is shown that the low energy path is the H atom on the C atom linking B shifting onto the middle C *via* TS46 with an energy of 261.0 kJ/mol. It should be noted that the Gibbs free energy at 298.15 K of the product IM83 is slightly higher than that of TS46 by 1.4 kJ/mol. However, the energy obtained in the geometry optimizations of B3PW91/6-311G(d,p) is 5.4 kJ/mol lower. This is understandable because the stationary points from G3MP2 and B3PW91 could be different and the entropy or the thermal correction of the energies for an IM and a TS would be different. The path in which the H atom on the methyl group conducting a 1,3-H-shift to form IM77 *via* TS47 lies 8.9 kJ/mol higher than the low energy path. IM79 may also conduct two other isomerization reactions: the H atom on the CH_3 terminal shifting onto the B atom with a Cl shifting onto the neighboring C simultaneously *via* TS44 with an energy of 295.2 kJ/mol, and the H located on the middle C shifting onto the C linked with B *via* TS42 with an energy barrier of 329.2 kJ/mol. Additionally, HCl, CH_4 and H_2 can be dissociated from IM79. By passing TS49 with a barrier of 287.8 kJ/mol, a four-member ring product (IM54) is formed. By converting IM79 into IM6, an energy of 383.9 kJ/mol is required. TS43 and TS48 link the same reactant (IM79) and product (IM48 + H_2) with barriers of 373.6 and 424.1 kJ/mol, respectively. IM49 is the product of a H_2 released from the CH_3 terminal in IM79 *via* TS41 with a barrier of 418.6 kJ/mol. The homogenous bond-cleavages without passing TS are also shown in Fig. 5a. The energies range from 325.9 to 469.3 kJ/mol. For all the direct reactions, the barriers or energies are above 261.0 kJ/mol.

IM79 can be attacked by either H or Cl radical in the system with very small barriers as shown in Fig. 5b and c. TS61, TS60 and TS59 in Fig. 5b are the transition states of releasing a H_2 molecule from IM79 if it is attacked by H radical. The energies are 52.7, 67.2 and 68.1 kJ/mol. If the terminal methyl group is attacked by H, a CH_4 molecule is released and the IM8 radical is remained. Compared with the dissociation of H, the barrier, 192.7 kJ/mol, of dissociating CH_3 is higher. Figure 5c shows IM79 being attacked by Cl. IM79 may decompose into IM58 + HCl *via* TS56 with an energy of 30.4 kJ/mol or into IM8 + CH_3Cl *via* TS57 with an energy of 184.9 kJ/mol. Obviously, IM58 radical is the ongoing reactant in the next step.

3.3.5 Decomposition of IM58 radical

Figure 6 shows the decomposition paths of IM58 radical. The isomerization, the radical (H, CH_3 or Cl) and HCl molecule releasing could be conducted. The lowest energy path is that the H on the middle C atom decomposes from IM58 without passing transition state with an energy of 121.9 kJ/mol. The dissociation of a CH_3 radical *via* TS34 needs 17.1 kJ/mol more. The rate branching ratio is 9.9×10^2. The energy, 294.4 kJ/mol, of decomposing a Cl from the BCl_2 terminal of IM58 is much higher. IM58 could also close its carbon chain associated with the H on the terminal methyl group being dissociated to form IM51 *via* TS33 with an energy of 295.2 kJ/mol. On the right hand side of Fig. 6, the transition states (TS32, TS31, TS30, TS38, TS36, TS35) and the energy barriers (174.1, 192.4, 200.1, 203.3, 253.1 and 318.6 kJ/mol) that link IM58 radical and its respective isomers (IM57, IM60, IM59, IM63, IM62 and IM61) are shown. All the isomers are the products of H shift except for IM63 and IM59, which are the products of the Cl on the B atom shifting onto the neighboring C atom. IM58 may also decompose into a four-member ring product of IM46 and an HCl molecule *via* TS37 with a high barrier of 349.8 kJ/mol. Therefore, the decomposition of the next step starts from IM50.

3.3.6 Decomposition of IM50 intermediate

Figure 7 is for the decomposition pathways of CH_3CCBCl_2 (IM50). Figure 7a shows the homogenous bond-cleavages and the Cl shifting reaction. The dissociation of an H atom needs a higher energy of 345.4 kJ/mol. The decomposition of a Cl atom or a CH_3 radical needs even higher energies by 455.1 and 490.7 kJ/mol, respectively. IM50 may also convert into a three-member ring IM52 *via* TS27 with an energy of 380.8 kJ/mol through a 1,2-Cl-shift process. Figure 7b is for the decomposition of IM50 attacked by H radical. The H, Cl atom or the CH_3 group could be dissociated (*via* TS39, TS29 and TS40) with the release of H_2, HCl and CH_4 molecule. The energies are 55.9, 119.2 and 208.9 kJ/mol. Figure 7c shows the decomposition of IM50 attacked by Cl. The decomposition of the CH_3 group to form IM5 and a CH_3Cl molecule *via* TS28 needs an energy of 256.5 kJ/mol. Therefore, the lowest energy path is to decompose an H in IM50 attacked by H with the formation of IM37 and H_2. IM37 is the reactant of the next step.

3.3.7 Decomposition of IM37 radical

Figure 8 shows the decomposition paths of the IM37 radical. The isomerization, the radical (Cl or H) and the molecule (HCl or H_2) releasing could be proceeded. The lowest energy path is that IM37 transforms into a three-member ring (IM40) *via* TS21 with an energy barrier of 215.1 kJ/mol. The Cl on the BCl_2 group could shift onto the neighboring C atom (*via* TS19) or onto the terminal C (*via* TS13) with energies of 289.0 kJ/mol and 317.3 kJ/mol. The dissociation of Cl or H atom from IM37 without passing a transition state needs an energy of 321.4 or 398.4 kJ/mol, respectively. An HCl molecule could be released *via* TS17 with an energy of 350.6 kJ/mol to form a

linear intermediate IM26. Both of the H atoms on the terminal $-CH_2$ group could be decomposed *via* TS18 to form IM23 and a H_2 molecule with an energy barrier of 394.9 kJ/mol. Accordingly, the decomposition of the next step starts from IM40.

3.3.8 Decomposition of IM40 radical

As shown in Fig. 9, the decomposition of IM40 has three types of reactions: intra-molecular H or Cl shift, the dissociation of an H or a Cl radical and the release of an HCl molecule. Among those, the lowest energy path is the H on the C atom shifting onto the neighboring C *via* TS24 to produce IM44 with an energy of 131.6 kJ/mol. The H shifts onto the other C atom *via* TS20 needs 58.6 kJ/mol more. The Cl shifting reaction *via* TS23 to form IM43 has an energy barrier of 328.9 kJ/mol. On the left hand side of the figure, the H and Cl radical releasing reactions need energies of 172.3 and 347.7 kJ/mol, respectively. An HCl molecule could also be dissociated form IM40 *via* TS22 to form IM27, but the barrier is 380.1 kJ/mol. The branching ratio of the reaction rate is 1.4×10^7 for the lowest energy path *via* TS24 with respect to the next lowest one (IM40 → IM29 + H). As a result, IM44 is the reactant of the next step.

3.3.9 Decomposition of IM44 radical

Figure 10 is for the decomposition pathways of IM44. Three reactions were found and the lowest one is that the H on the C atom shifts onto the C linking BCl_2 *via* TS26 to produce IM45 with an energy barrier of 173.2 kJ/mol. IM44 may also release H or Cl radical without passing any transition state to form IM29 and IM35. The energies are 255.7 and 369.8 kJ/mol, respectively. Obviously, IM45 is the reactant of next step.

3.3.10 Decomposition of IM45 radical

Figure 11 presents the decomposition paths of IM45. The lowest energy path is that the linear C chain in IM45 bends and forms an isomer IM42 *via* TS25 with a barrier of 192.1 kJ/mol. The Cl atom in the BCl_2 group could shift onto the neighboring C *via* TS16 with an energy barrier of 278.9 kJ/mol. On the left side of the figure, three paths to dissociate a Cl and two H radicals to produce IM34 + Cl, IM28 + H and IM30 + H are shown. The respective energies are 324.4, 381.2 and 411.6 kJ/mol without transition state. So, the next step will be the decomposition of IM42.

3.3.11 Decomposition of IM42 radical

Figure 12 demonstrates the decomposition pathways of IM42 by releasing an H or a Cl radical and a H_2 molecule. The lowest energy path is to dissociate the H on the C atom linking the BCl_2 group to form IM29 with an energy of 148.5 kJ/mol. Decomposing a Cl atom needs 42.0 kJ/mol more. The release of the other H atom in IM42 requires a higher energy of 224.1 kJ/mol. Actually, a H_2 molecule could also be released *via* TS15 with an even higher energy barrier of 338.2 kJ/mol. The rate branching ratio is 2.3×10^7 for the lowest energy reaction (IM42 → IM29 + H) with respect to the next lowest energy path (IM42 → IM36 + Cl). Therefore, intermediate IM29 is the ongoing reactant in the next step.

3.3.12 Decomposition of IM29 intermediate

Figure 13 shows the decomposition pathways of C_3HBCl_2 (IM29). Figure 13a is for the Cl shifting, the HCl molecule releasing and the homogenous bond-cleavages reactions. The path that the Cl atom in the BCl_2 group shifts onto the C atom linked with an H atom *via* TS10 has a high energy barrier of 265.8 kJ/mol. Dissociating an HCl molecule from IM29 to produce IM13 needs a higher energy of 351.4 kJ/mol. The energies of the homogenous bond-cleavage reactions as shown in the left hand side of the figure are more than 408.1 kJ/mol. For the H and Cl radical attacking reactions as shown in Fig. 13b–c, the energy barriers are much lower. The one for H attacking is 82.2 kJ/mol to produce IM24 *via* TS14 and that for the Cl attacking is only 44.0 kJ/mol to produce IM24 *via* TS12. The rate branching ratios is 4.9×10^6 for the lowest energy path. Thus, IM24 is the reactant in the next step.

3.3.13 Decomposition of IM24 radical

Figure 14 illustrates the decomposition paths of IM24 radical for the isomerization and the Cl dissociation reactions. The lowest energy path is that the three-member ring of the C atoms opens to form a more stable intermediate IM23 *via* TS7 with an energy of 64.3 kJ/mol. IM24 may also dissociate a Cl atom to form IM15 without passing a transition state but needs much higher energy of 383.8 kJ/mol. The next step will start from IM23.

3.3.14 Decomposition of IM23 radical

Figure 15 shows the decomposition paths of IM23 for Cl shift and Cl release reactions. The lowest energy path is that a Cl atom in the BCl_2 group shifts onto the neighboring C atom *via* TS6 with an energy of 185.3 kJ/mol. The Cl shifting onto the terminal C atom *via* TS5 needs 49.6 kJ/mol more. The energy for the Cl dissociation reaction without passing transition state is 380.2 kJ/mol, and the product is a linear intermediate IM12. The branching ratio of the reaction rate is 4.9×10^8 for the lowest path (*via*

TS6) with respect to the next lowest energy one (*via* TS5) and IM18 is the reactant of the next step.

3.3.15 Decomposition of IM18 radical

Figure 16 demonstrates the decomposition paths of IM18 radical for its isomerization and Cl releasing reactions. The lowest energy path is that the three-member ring in IM18 transforms into a four-member ring in IM20 *via* TS3 with an energy barrier of 48.0 kJ/mol. The Cl on the C atom shifting onto the terminal C to form IM19 *via* TS2 needs a higher energy of 300.4 kJ/mol. On the left hand side of the figure, different sites of Cl atom in IM18 are dissociated to produce IM14 and IM16. The energies are 270.4 and 391.5 kJ/mol, respectively. Therefore, the decomposition of the next step starts from IM20.

3.3.16 Decomposition of IM20 radical

Figure 17 shows the decomposition pathways of IM20. The Cl dissociation and Cl shift reactions are involved. The lowest energy, 155.1 kJ/mol, path is to dissociate the Cl atom on the C atom without transition state. The release of the Cl on the B atom needs much higher energy of 365.7 kJ/mol. The Cl shift reactions are shown on the right hand side of the figure. The Cl atom either on the B atom or on the C atom could shift onto the neighboring C atom. These corresponds to IM22 (*via* TS4) and IM21 (*via* TS8) with the energy barriers of 175.8 and 219.1 kJ/mol, respectively. The rate branching ratio is 4.2×10^3 for the lowest energy path (IM20 $\rightarrow$ IM13 + Cl) with respect to the next lowest one (*via* TS4). Thus, IM13 is the reactant of the next step.

3.3.17 Decomposition of IM13 intermediate

Figure 18 is for the decomposition paths of intermediate IM13, which is also the last reactant to produce a C_3B cluster. Figure 18a presents the direct decomposition reactions of IM13. It shows that either the Cl shift (to form IM17 *via* TS1) or the Cl release (to form C_3B) reaction requires quite high energy by 481.7 or 499.2 kJ/mol, respectively. However, Fig. 18b shows that the dissociation of the last remaining Cl atom *via* TS9 needs a barrier of only 154.0 kJ/mol by H attacking. Therefore, the C_3B cluster in $^2A_1$ state with C_{2v} symmetry is the ultimate product of the lowest energy pathway of the C_3H_6 (propene) $+BCl_3 + H_2$ pyrolysis system.

3.4 Proposal of the lowest paths

According to the discussions of this paper, one of the possible lowest reaction pathways can be drawn. The initialization of the reaction chain is the production of the H radical from propene [67] and the Cl radical from IM99 (a dot will be used to emphasize the species being a radical)

(1) $C_3H_6 \rightarrow C_3H_6^*(a^3A) \rightarrow$ TS58 $\rightarrow$ H· + IM74(C_3H_5·)
(2) IM99 $\rightarrow$ IM91 + Cl·.

The respective energy barriers (Gibbs free energies) in reaction (1) are 270.2 and 148.7 kJ/mol at 298.15 K [67], and the energy for IM99 decomposing into IM91 and Cl radical in (2) is 303.3 kJ/mol. But for temperature at 1,200 K, the energy for reaction (2) decreases into 179.5 kJ/mol and those for reaction (2) change to 233.9 and 153.4 kJ/mol. These energies at any other temperatures can also be obtained with classical thermodynamics by using the data listed in the supplementary materials. It should be noted that the production of H radical by direct decomposition of propene at 1,200 K needs a smaller energy of 226.2 kJ/mol, which is even smaller than that in the electronic excitation as presented in Ref. [67]. Therefore, the production of the radicals (H and Cl) at 1,200 K should be

(1) $C_3H_6 \rightarrow$ H· + IM74(C_3H_5·) (with 226.2 kJ/mol)
(1') $C_3H_6 \rightarrow C_3H_6^*(a^3A) \rightarrow$ TS58 $\rightarrow$ H· + IM74(C_3H_5·) with 233.9 and via TS58 with 153.4 kJ/mol
(2) IM99 $\rightarrow$ IM91 + Cl· (with 179.5 kJ/mol).

The ongoing lowest reaction pathways, in which the reaction in each step has the lowest energy barrier or the lowest energy, of the $C_3H_6 + BCl_3 + H_2$ pyrolysis system are shown in Fig. 19 ['(a)' for 298.15 K and '(b)' for 1,200 K].

The chemical reactions are (TS, energy or energy barriers at 298.15 K are shown in the parentheses following each reaction)

(3) $C_3H_6 + BCl_3 \rightarrow$ IM99 (via TS76 with 125.6 kJ/mol)
(4) IM99 + Cl· $\rightarrow$ IM85 + HCl (via TS85 with 25.8 kJ/mol)
(5) IM85 $\rightarrow$ IM79 + Cl· (with 60.6 kJ/mol)
(6) IM79 + Cl· $\rightarrow$ IM58 + HCl (via TS56 with 30.4 kJ/mol)
(7) IM58 $\rightarrow$ IM50 + H· (with 121.9 kJ/mol)
(8) IM50 + H· $\rightarrow$ IM37 (via TS39 with 56.0 kJ/mol)
(9) IM37 $\rightarrow$ IM40 (via TS21 with 215.1 kJ/mol)
(10) IM40 $\rightarrow$ IM44 (via TS24 with 131.6 kJ/mol)
(11) IM44 $\rightarrow$ IM45 (via TS26 with 173.2 kJ/mol)
(12) IM45 $\rightarrow$ IM42 (via TS25 with 192.1 kJ/mol)
(13) IM42 $\rightarrow$ IM29 + H· (with 148.5 kJ/mol)
(14) IM29 + Cl· $\rightarrow$ IM24 + HCl (via TS12 with 44.0 kJ/mol)
(15) IM24 $\rightarrow$ IM23 (via TS7 with 64.3 kJ/mol)
(16) IM23 $\rightarrow$ IM18 (via TS6 with 185.3 kJ/mol)

(17) IM18 → IM20 (via TS3 with 48.0 kJ/mol)
(18) IM20 → IM13 + Cl· (with 155.1 kJ/mol)
(19) IM13 + H· → C_3B + HCl
(via TS9 with 154.0 kJ/mol).

It is shown that all the energy barriers are not more than 215.1 kJ/mol. The values are moderate for the gas phase pyrolysis reactions. The highest energy step is that IM37 transforms into the three-member ring IM40 with an energy of 215.1 kJ/mol in reaction (9). The higher energy steps are reactions (11), (12), (16), (18) and (19) corresponding to the energies in the region of 150–200 kJ/mol by 173.2, 192.1, 185.3, 155.1 and 154.0 kJ/mol.

For temperature at 1,200 K, the respective energies for reactions (3–19) are 275.1, 50.9, −50.1, 125.0, 11.9, 136.7, 239.5, 135.5, 172.9, 203.5, 45.9, 127.9, 73.9, 191.9, 70.9, 52.9 and 247.6 kJ/mol. It should be noted that reactions (3), (9), (12) and (19) have energies higher than 200 kJ/mol by 275.1, 239.5, 203.5 and 247.6 kJ/mol, respectively. It is also noted that all the energies of the radical attacking reactions [except reaction (4)] increased more than 80.0 kJ/mol [i.e., reactions (6), (8), (14) and (19)] mainly due to a negative entropy change of the reaction. But the energy at 1,200 K for isomerization reactions [i.e., reactions (9), (10), (11), (12), (15), (16) and (17)] remains almost unchanged (or not more than 23.0 kJ/mol) mainly due to an unchanged entropy of the reaction. It is also interesting that the energies of radical releasing reactions (5), (7), (13) and (18) decreased more than 100.0 kJ/mol (i.e., from 60.6 to −50.1, 121.9 to 11.9, 148.5 to 45.9, 155.1 to 52.9 kJ/mol) benefited from a positive entropy change of the reaction. Therefore, the highest energy barrier of the lowest paths is 275.1 kJ/mol at 1,200 K.

4 Conclusions

A kinetic research on the gas phase reaction pathways of C_3H_6-BCl_3-H_2 system was carried out theoretically. A total number of 95 transition states and 103 intermediates in the system were obtained with density functional theory at B3PW91/6-311G(d,p) level. The intrinsic reaction coordinates were calculated with the same method to confirm the linked profiles. Molecular energies were evaluated with the high accurate model chemistry method at G3(MP2) level after a non-dynamical correlation diagnosis with the dominant configuration coefficient of a complete active space self-consistent field (CASSCF) calculation. Heat capacity, entropy, enthalpy and Gibbs free energy corrections at 298.15 K were calculated with standard statistical thermodynamics by using the optimized geometries and the scaled theoretical frequencies. The heat capacities (as a function of temperature) were calculated statistically and fitted into polynomials, which can be used in the high temperature evaluations of the Gibbs free energies classically.

Potential energy surface profiles of the C_3H_6-BCl_3-H_2 pyrolysis system including direct decompositions and the radical attacking reactions were illustrated in the order of gradual decompositions. The energy barriers or the reaction energies were examined by using the Gibbs free energies at 298.15 K. It was found that the lowest energy paths are mainly in the radical attacking chain reactions. There were 19 reaction steps in the lowest paths including two steps to produce H and Cl radicals. The lowest decompositions paths were proposed as: C_3H_6 + BCl_3 → IM99 → IM85 → IM79 → IM58 → IM50 → IM37 → IM40 → IM44 → IM45 → IM42 → IM29 → IM24 → IM23 → IM18 → IM20 → IM13 → C_3B. The respective energy barriers are 125.6, 25.8, 60.6, 30.4, 121.9, 56.0, 215.1, 131.6, 173.2, 192.1, 148.5, 44.0, 64.3, 185.3, 48.0, 155.1 and 154.0 kJ/mol at 298.15 K. For a typical temperature (1,200 K) adopted in the experiments, the energies change into 275.1, 50.9, −50.1, 125.0, 11.9, 136.7, 239.5, 135.5, 172.9, 203.5, 45.9, 127.9, 73.9, 191.9, 70.9, 52.9 and 247.6 kJ/mol. These data indicated that the decomposition paths are feasible in the experimental condition.

Acknowledgments Part of the calculations was performed in the High Performance Computation Center of the Northwestern Polytechnical University. Supports by the National Natural Science Foundation of China (No. 50572089 and 50642039) and the Chinese 973 Fundamental Researches are greatly acknowledged.

References

1. Cox BN, Zok FW (1996) Solid State Mater Sci 1:666
2. Halbig MC, Brewer DN, Eckel AJ (1997) NASA/TM. New York Press, New York
3. Naslain R (2004) Compos Sci Technol 64:155
4. Cutard T, Huger M, Fargeot D (1993) In: Naslain R (ed) Proc of HT–CMC1. Woodhead, Abington Cambridge, pp 33–49
5. Schmidt S, Beyer S, Knabe H, Immich H, Meistring R, Gessler A (2004) Acta Astronaut 55:409
6. Cheng LF, Xu YD, Zhang LT, Yin XW (2002) J Mater Sci 37:5339
7. Kobayashi K, Maeda K, Sano H, Uchiyama Y (1995) Carbon 33:397
8. Cheng LF, Xu YD, Zhang LT, Gao R (2001) Carbon 39:1127
9. Tsou HT, Kowbel W (1995) Carbon 33:1289
10. Schulte-Fischedick J, Schmidt J, Tamme R, Kröner U, Arnold J, Zeiffer B (2004) Mater Sci Eng A 386:428
11. Isola C, Appendino P, Bosco F, Ferraris M, Salvo M (1998) Carbon 36:1213
12. Naslain R, Guette A, Rebillat F, Pailler R, Langlais F, Bourrat X (2004) J Solid State Chem 177:449
13. Jung CH, Lee MJ, Kim CJ (2004) Materials Letters 58:609
14. Chao MJ, Niu X, Yuan B, Liang EJ, Wang DS (2006) Surface & Coatings Technology 201:1102
15. Vincent H, Vincent C, Berthbt MP, Bouix J, Gonzalez G (1996) Carbon 34:1041

16. Nakajima T, Koh M, Katsube T (2000) Solid State Sciences 2:17
17. Hach CT, Jones LE, Crossland C, Thrower PA (1999) Carbon 37:221
18. Koh M, Nakajima T (1998) Carbon 36:913
19. Schouler MC, Cheynet MC, Sestier K, Garden J, Gadelle P (1997) Carbon 35:993
20. Berjonneau J, Langlais F, Chollon G (2007) Surface & Coatings Technology 201:7273
21. Stinton DP, Besmann TM, Lowden RA (1988) Amer Ceram Soc Bull 67:369
22. Way BM, Dahn JR, Tiedje T, Myrtle K, Kasrai M (1992) Phys Rev B 46:1697
23. Cermignani W, Paulson TE, Onneby C, Pantano CG (1995) Carbon 33:367
24. Derre A, Filipozzi L, Peron F (1993) J Phys IV 3(C3):195
25. Jacques S, Guette A, Bourrat X, Langlais F, Guimon C, Labrugere C (1996) Carbon 34:1135
26. Kouvetakis J, Sasaki T, Shen C, Hagiwara R, Lerner M, Krishana KM (1989) Synthetic Met 34:1
27. Jansson U, Carlsson JO, Stridh B, Soederberg S, Olsson M (1989) Thin Solid Films 172:81
28. Oliveira JC, Conde O (1997) Thin Solid Films 307:29
29. Zeng Y, Su KH, Deng JL, Wang T, Zeng QF, Cheng LF, Zhang LT, Xu YD (2008) J Mol Struct (THEOCHEM) 861:103
30. Liu YS, Zhang LT, Cheng LF, Zeng QF, Zhang WH (2009) Applied Surface Science 255:5729
31. Yang WB, Zhang LT, Cheng LF, Liu YS, Xu YD (2007) Acta Materiae Compos Sin 24:103
32. Yang WB, Zhang LT, Liu YS, Cheng LF, Zhang WH (2007) Appl Compos Mater 14:277
33. Liu YS, Zhang LT, Cheng LF, Yang WB, Xu YD (2009) Applied Surface Science 255:8761
34. Wang T, Su KH, Deng JL, Zeng Y, Zeng QF, Cheng LF, Zhang LT (2008) Theor Compu Chem 7:1269
35. Joly A, Hebd CR (1883) Seances Acad Sci 97:456
36. Frisch MJ, Trucks GW, Schlegel HB, Scuseria GE, Robb MA, Cheeseman JR, Zakrzewski VG, Montgomery Jr JA, Stratmann RE, Burant JC, Dapprich S, Millam JM, Daniels AD, Kudin KN, Strain MC, Farkas O, Tomasi J, Barone V, Cossi M, Cammi R, Mennucci B, Pomelli C, Adamo C, Clifford S, Ochterski J, Petersson GA, Ayala PY, Cui Q, Morokuma K, Salvador P, Dannenberg JJ, Malick DK, Rabuck AD, Raghavachari K, Foresman JB, Cioslowski J, Ortiz JV, Baboul AG, Stefanov BB, Liu G, Liashenko A, Piskorz P, Komaromi I, Gomperts R, Martin RL, Fox DJ, Keith T, Al-Laham MA, Peng CY, Nanayakkara A, Challacombe M, Gill PMW, Johnson B, Chen W, Wong MW, Andres JL, Gonzalez C, Head-Gordon M, Replogle ES, Pople JA (2003) Gaussian Inc. Pittsburgh
37. Becke AD (1993) J Chem Phys 98:5648
38. Burke K, Perdew JP, Wang Y (1998) In: Dobson JF, Vignale G, Das MP (Eds.) Electronic density functional theory: recent progress and new directions. Plenum Press, New York
39. Su KH, Wei J, Hu XL, Yue H, Lu L, Wang Y, Wen ZY (2000) Acta Physiologica Chimica Sinica 16:643
40. Su KH, Wei J, Hu XL, Yue H, Lu L, Wang Y, Wen ZY (2000) Acta Physiologica Chimica Sinica 16:718
41. http://www.bsc.ustc.edu.cn/~dxl/gaussian/VFS.mht
42. Garrett BC, Truhlar DG (1983) J Phys Chem 87:4553
43. Hegarty D, Robb MA (1979) Mol Phys 38:1795
44. Eade RHA, Robb MA (1981) Chem Phys Lett 83:362
45. Schlegel HB, Robb MA (1982) Chem Phys Lett 93:43
46. Bernardi F, Bottini A, McDougall JJW, Robb MA, Schlegel HB (1984) Far Symp Chem Soc 19:137
47. Yamamoto N, Vreven T, Robb MA, Frisch MJ, Schlegel HB (1996) Chem Phys Lett 250:373
48. Frisch MJ, Ragazos IN, Robb MA, Schlegel HB (1992) Chem Phys Lett 189:524
49. Curtiss LA, Redfern PC, Raghavachari K, Rassolov V, Pople JA (1999) J Chem Phys 110:4703
50. Baboul AG, Curtiss LA, Redfern PC, Raghavachari K (1999) J Chem Phys 110:7650
51. Wang SK, Zhang QZ, Gu YS (2004) Acta Chim Sinica 62:550
52. Koch LC, Marshall P, Ravishankara AR (2004) J Phys Chem A 108:5205
53. Curtiss LA, Raghavachari K, Redfern PC (1997) J Chem Phys 106:1063
54. Curtiss LA, Redfern PC, Raghavachari K (1998) J Chem Phys 109:42
55. Kevill DN, Rissmann TJ (1986) J Cryst Growth 74:210
56. Moss TS (1995) PhD Thesis, Georgia Institute of Technology. Atlanta
57. Moss TS, Lackey WJ, More KL (1998) J Am Ceram Soc 81:3077
58. Hannache H, Langlais F, Naslain R (1985) Proceedings of the Fifth European Conference on Chemical Vapour Deposition. Uppsala University, Department of Chemistry, Uppsala
59. Berjonneau J, Chollon G, Langlais F (2006) J Electrochem Soc 153:795
60. (2008). http://webbook.nist.gov/chemistry/
61. Chase Jr MW (1998) J Phys Chem Ref Data, Monograph No. 9
62. Lide DR (1996–1997) Section 5: thermochemistry, electrochemistry, and kinetics. CRC Handbook of Chemistry and Physics, 77th edn. CRC Press, New York
63. Lias SG, Bartmess JE, Liebman JF, Holmes JL, Levin RD, Mallard WG (1998) J Phys Chem Ref Data, (Suppl. 1):45
64. Schlegel HB, Stephen JH (1994) J Phys Chem 98:11178
65. Yao XP, Su KH, Wang X, Zeng QF, Cheng LF, Xu YD, Zhang LT (2007) Comput Mat Sci 40:504–524. Erratum (2008) Comput Mat Sci 44:838
66. Wigner EP, Witmer EE (1928) Z Phys 51:859
67. Qu YN, Su KH, Wang X, Zeng QF, Cheng LF, Zhang LT (2010) J Comput Chem. doi:10.1002/jcc